NUMERICAL INVESTIGATION INTO THE EFFECTS OF PERIPHERAL WINDSCREENS ON AIR-COOLED CONDENSER FAN PERFORMANCE UNDER WINDY CONDITIONS

Adam VENTER[1], Michael OWEN[1] and Jacques MUIYSER[2]

[1]*Solar Thermal Energy Research Group (STERG), University of Stellenbosch, South Africa*
[2]*Dept. of Mechanical and Mechatronic Engineering, University of Stellenbosch, South Africa*

Keywords: Air-cooled condensers, Windscreens, Axial fan models, ANSYS Fluent

ABSTRACT: The performance of air-cooled condensers (ACCs) is highly sensitive to ambient wind conditions. In a forced-draft configuration, wind induces flow distortions across the fan inlet regions and as a result, the volumetric effectiveness of the fans suffer proportionately. Porous peripheral windscreens are commonly implemented as a strategy to alleviate wind effects. However, uncertainty surrounds the impacts of this measure. In this study, a computational fluid dynamics (CFD) model, replicating an experimental fan row test facility with interchangeable peripheral windscreens is created and validated against experimental results. For the particular case investigated, which is representative of an ACC of low platform height, the windscreens primarily degrade the volumetric effectiveness of the fan row, up to a maximum performance deficit of 19% at an approximated full-scale wind speed of 10 m/s.

1 INTRODUCTION

Maulbetsch *et al.* (2011) recognize the effects of wind to be the most significant challenge facing air-cooled condenser (ACC) performance. Wind causes an exacerbated maldistribution of the airflow at the fan inlet regions, augmenting separation around the fan shrouds (Meyer, 2004) and off-axis inflow (Stinnes and von Backström, 2002). Consequently, multiple attempts to mitigate adverse wind effects have been effected, of which one such implementation is the installation of porous peripheral windscreens along the perimeter of the ACC fan platform. The windscreens attempt to improve volumetric flow through fan units by reduction of these airflow distortions.

However, little is known about the mechanisms that determine the effect of windscreens on ACC performance and there exists considerable uncertainty in the literature regarding the benefit of this measure (Marincowitz, 2018). Maulbetsch and DiFilippo (2016) attest that this uncertainty is due, in part, to a lack of consistent field and/or experimental data against which prior numerical models could be concretely validated. In recognition of this deficiency, Marincowitz (2018) modified an experimental ACC fan row test facility to incorporate peripheral windscreens and a controllable cross-flow (wind) induction capability, with a motivation to remedy the lack of experimental data against which a numerical model could be validated. The aim of this study is, therefore, to use the experimental results of Marincowitz (2018) to validate a numerical model that can be confidently used to further the understanding of the mechanisms that determine the effect of windscreens on ACC fan performance. The scope of this study is limited to the numerical replication of the experimental analysis, so as to

concretely validate the numerical modelling approach through a detailed comparison to the controlled experiment.

2 EXPERIMENTAL FACILITY SIMULATIONS

Marincowitz's (2018) experimental facility consists of three 630 mm diameter fan tunnels, constructed according to ISO 5801 type B standard (ISO, 2007), representing an internal fan row of a forced-draft ACC. All three fan tunnels use the so-called L2-fan with 8 blades and a midsection solidity of 0.532, further details of which are provided by Augustyn (2013). Marincowitz (2018) introduced a controllable cross-flow by ducting exhaust flow from an open-loop wind-tunnel past the fan row, and modular construction of the different ducting segments allowed for installation and removal of windscreen material at the upwind peripheral inlet to the fan row. With respect to dimensionless platform height, the experimental facility is geometrically similar to an operating ACC with retractable windscreens for which full-scale test data is available in Maulbetsch and DiFilippo (2016). Marincowitz (2018) was able to achieve close correspondence between the facility's performance and that of the full-scale field measurements.

The experimental facility of Marincowitz (2018) is numerically simulated using the computational fluid dynamics (CFD) code, ANSYS Fluent. Fluent employs a finite volume formulation for iterative solution of the Reynolds Average Navier-Stokes equations. Turbulence modelling is augmented by adoption of the realizable k-ε turbulence model (Shih *et al.*, 1995). The realizable k-ε turbulence model is chosen here based on the favourable performance it offers in combination with the implicit fan models this study utilizes (van der Spuy, 2011). Furthermore, the SIMPLE pressure-velocity coupling algorithm and least-squares cell-based gradient calculation scheme are used.

The numerical geometry, shown in Fig. 1, resembles the internal dimensions of Marincowitz's (2018) experimental facility, plus the inclusion of an exhaust outlet air space and a portion of the coupled wind-tunnel. The outlet air space is extended over the third tunnel in the fan row so that the imposed boundary conditions do not influence the flow field exiting the fan row.

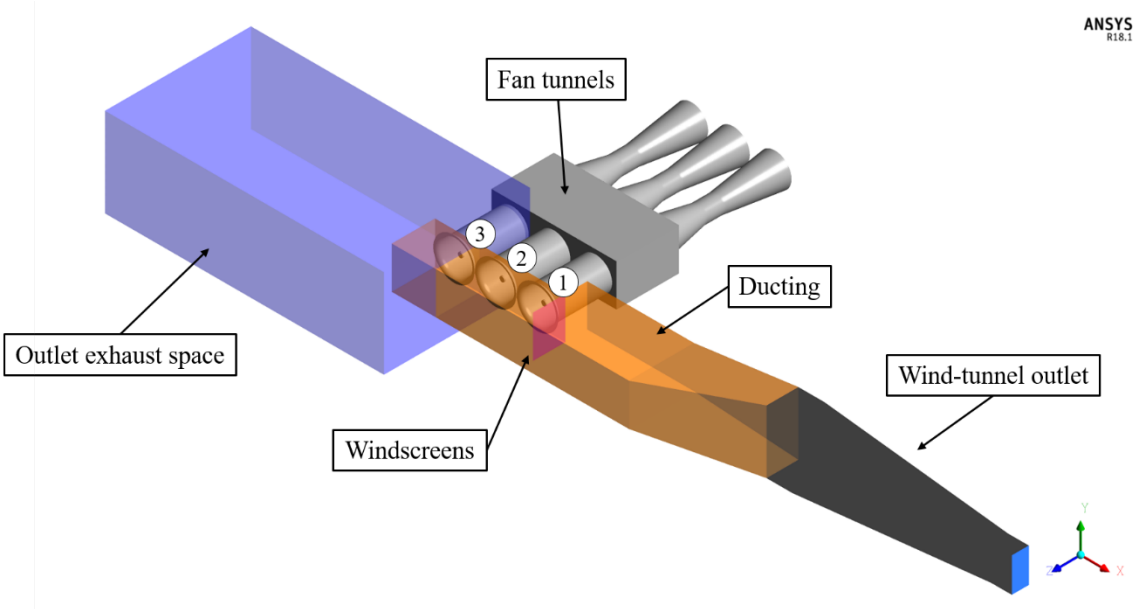

Figure 1: Numerical domain of experimental ACC fan row test facility with peripheral windscreens

A mass flow inlet is prescribed to establish the desired cross-flow condition, while loss coefficients specified at the fan tunnel outlets are set such that under ideal inlet flow conditions, the individual fans' operating points, $\dot{V}_{ideal}$, of 1.45 m^3/s (Fourie, 2014) would be realizable.

The windscreens are incorporated into the numerical simulations by effecting an equivalent pressure drop in place of the physical structure. Implementation of such implicit pressure drop conditions is achievable in ANSYS Fluent through the use of the porous-jump boundary condition. This boundary condition introduces an empirically determined flow resistance into the governing momentum equations as an added sink term. In this case, the porous-jump condition is configured to replicate the resistance characteristics of a 50% solidity windscreen material and is applied to infinitely thin faces spanning across the upwind peripheral inlet of the fan row.

2.1 Axial Fan Models

This study utilizes both the pressure jump method (PJM) and the extended actuator disk method (EADM) of van der Spuy (2011) in its numerical representation of the facility's axial flow fans. With the PJM, the effect of the fan is incorporated through a discontinuous static pressure rise applied across the fan rotation plane. The static-to-static pressure rise corresponds to the velocity through the fan annulus and is added as a source term to the linear momentum equations of the CFD solver in the fan's axial direction. Thorough discussion of the PJM is provided by van der Spuy (2011). The EADM model effects the operation of an axial flow fan through a step-change in tangential and axial velocity in the flow field over the fan's plane of rotation. The step-change originates from forces calculated using blade element theory employing lift and drag coefficients determined through two-dimensional, isolated airfoil profile tests (van der Spuy, 2011). Consider the isolated two-dimensional airfoil profile in Fig. 2.

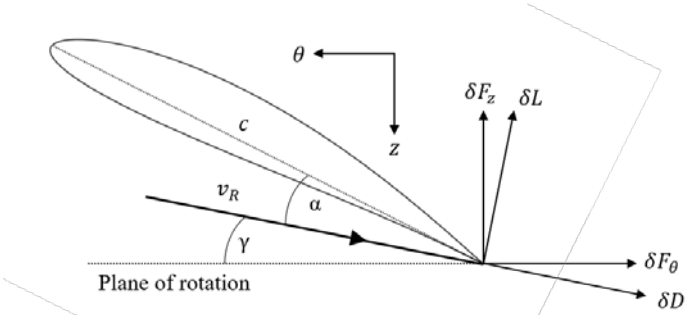

Figure 2: Radial fan blade element

The associated lift and drag forces at a radius r, as determined in the EADM formulation, are captured by Eq. (1) and Eq. (2).

$$\delta L = \frac{1}{2}\rho C_l |v_R^2| c \delta r \quad (1)$$

$$\delta D = \frac{1}{2}\rho C_d |v_R^2| c \delta r \quad (2)$$

Where ρ, C_l, C_d, c, δr is the density, lift coefficient, drag coefficient, chord length and radial thickness respectively. The average relative velocity vector, v_R, is determined based on velocities up- and downstream of the fan rotation plane. These forces are converted into the local axial and azimuthal directions, then likewise introduced into the flow field as volumetric

source terms in the linear momentum equations of the CFD solver, described by Eq. (3) and Eq. (4).

$$\frac{\delta F_z}{\delta V} = \frac{1}{2}\rho|v_R^2|\frac{\sigma}{t}(\delta L\cos\gamma - \delta D\sin\gamma) \quad (3)$$

$$\frac{\delta F_\theta}{\delta V} = \frac{1}{2}\rho|v_R^2|\frac{\sigma}{t}(\delta L\sin\gamma + \delta D\cos\gamma) \quad (4)$$

Where σ is the blade solidity and t the thickness of the computational cell. The EADM compensates for the inability of the actuator disk method (ADM) (Thiart and von Backström, 1993) to account for the presence of radial flow effects, characteristic of axial flow fan operation at low volumetric flow rates. At low flow rates, the occurrence of radial flow results in a three-dimensional flow regime which is analogous to flow through a mixed flow fan (Lewis, 1996). The radial shift of a fluid particle during its passage over a fan blade uncovers an additional work contribution known as the Coriolis force (Lewis, 1996). The Coriolis force effects a greater load exertion on the flow field which the EADM accounts for through modification of the fan blade's numerically derived lift characteristics (van der Spuy, 2011).

For verification of the employed axial fan models' construction and implementation, a single fan tunnel from the experimental facility was simulated in isolation. The models' ability to predict the 630 mm L2 fan's static pressure characteristics, provided by Marincowitz (2018) and Fourie (2014) who modelled the same facility, was assessed and is shown in Fig. 3. Both the PJM and EADM models demonstrate the ability to closely predict fan performance at high flow rates, however, a marked underperformance of the EADM is witnessed at low flow rates. The underperformance of the EADM, in terms of static pressure prediction, at low flow rates is however expected (van der Spuy, 2011). The performance of the ADM has likewise been included in Fig. 3 to show the improved performance the EADM holds. For the full experimental facility simulations, the use of different fan model configurations for the three fan tunnels was trailed, however, the best experimental correlation is uncovered when using the EADM for representation of the upwind edge fan (fan 1) and the PJM for the two downwind fans (fan 2 and fan 3).

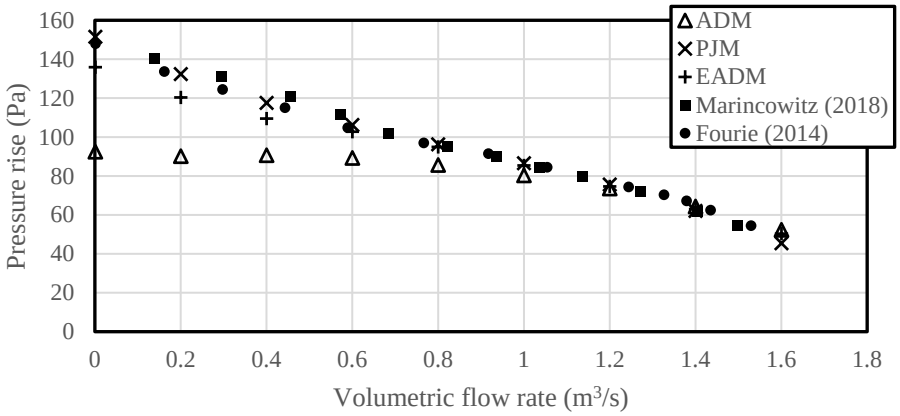

Figure 3: Axial fan model verification

3 VALIDATION OF THE NUMERICAL MODELING APPROACH

The resultant numerical model's ability to predict cross-flow and windscreen effects for different screen heights is evaluated. Screen height is referenced according to the percentage coverage of the peripheral inlet area, extending down from the platform height. The results of the validation cases are presented in Fig. 4, 5, 6 and 7. In all the tested cases, air at a density of

1.2 kg/m^3 and viscosity of 1.8×10^{-5} kg/ms feeds through the facility, with the fans operating at 1000 rpm. The numerical results are presented relative to their experimental counterparts as determined by Marincowitz (2018). Volumetric effectiveness ζ, described by Eq. (5), is captured relative to increasing cross-flow parameter β, described by Eq. (6). Cross-flow is made dimensionless by division of the average velocity beneath the fan platform, v_x, with fan blade tip speed, v_{tip}. A cross-flow of $\beta = 0.1$ represents an effective no-wind (nw) scenario. The cross-flow in this instance is induced solely by the suction of the fans.

$$\zeta = \dot{V}_{actual}/\dot{V}_{ideal} \quad (5)$$

$$\beta = v_x/v_{tip} \quad (6)$$

Marincowitz (2018) equated cross-flow to approximate wind speed at platform height, v_w, through Eq. (7). Where $\dot{V}_x$ is the volumetric cross-flow rate at each test point, $\dot{V}_f$ the flow rate through the fans and Hp the platform height. Derivation of the constants in Eq. 7 is available in Marincowitz (2018).

$$v_w = 10\left[\left(\dot{V}_x - \dot{V}_{nw}\right) + \sum_{i=1}^{3}\left(\dot{V}_{fi(nw)} - \dot{V}_{fi}\right)\right]/7H_p \quad (7)$$

In all the investigated cases, close correlation between the experimental and numerical results is witnessed for $\beta < 0.26$. However, the numerical results start to deviate from their experimental counterparts thereafter. The determined trends at the higher cross-flow rates, however, continue to primarily correspond to those of the experimental results. Deviation of the numerical results is attributed to the limitations of the axial fan models. For the edge fan, the lower fan flow rates coupled with high degrees of off-axis inflow and separation around the bellmouth intake potentially uncover additional energy transfer mechanisms that EADM ignores. Failure of the EADM to sufficiently entrain flow into the edge fan at the higher cross-flow rates is also possible cause for the lesser determined performance of the second fan, as underperformance of the edge fan encourages greater cross-flow velocities across the second fan, allowing separated flow around the second fan bellmouth intake to develop.

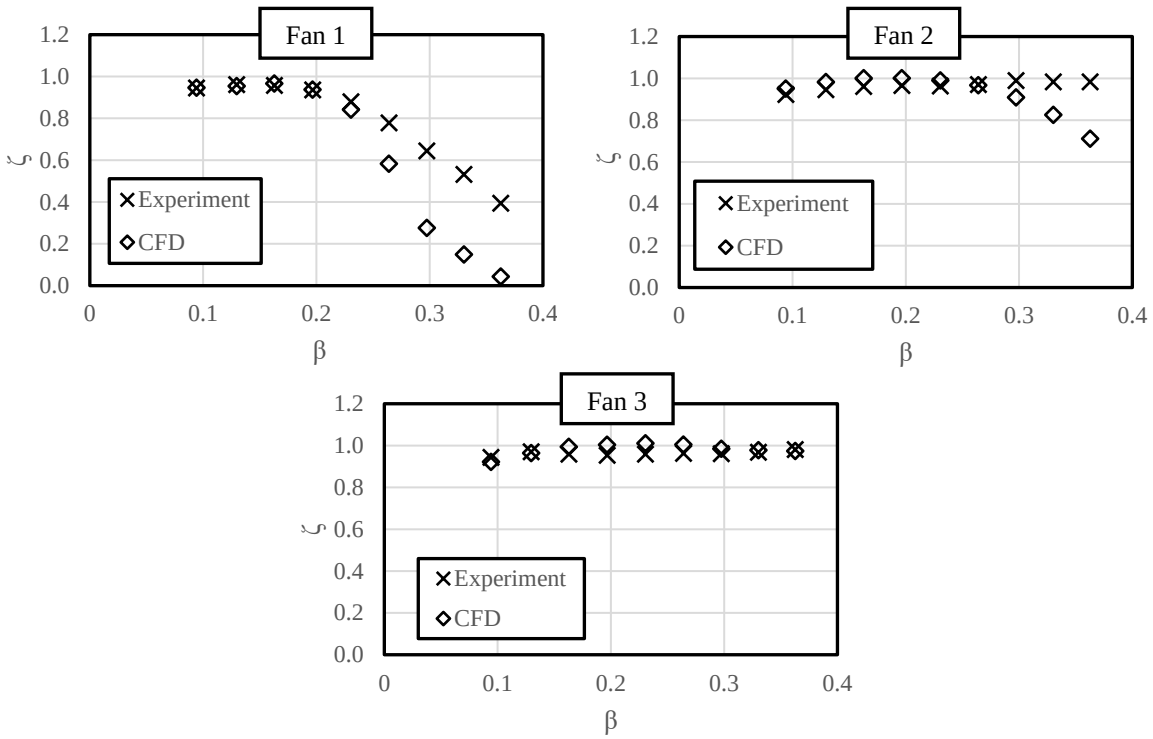

Figure 4: Effect of cross-flow on individual fan performance – No screen

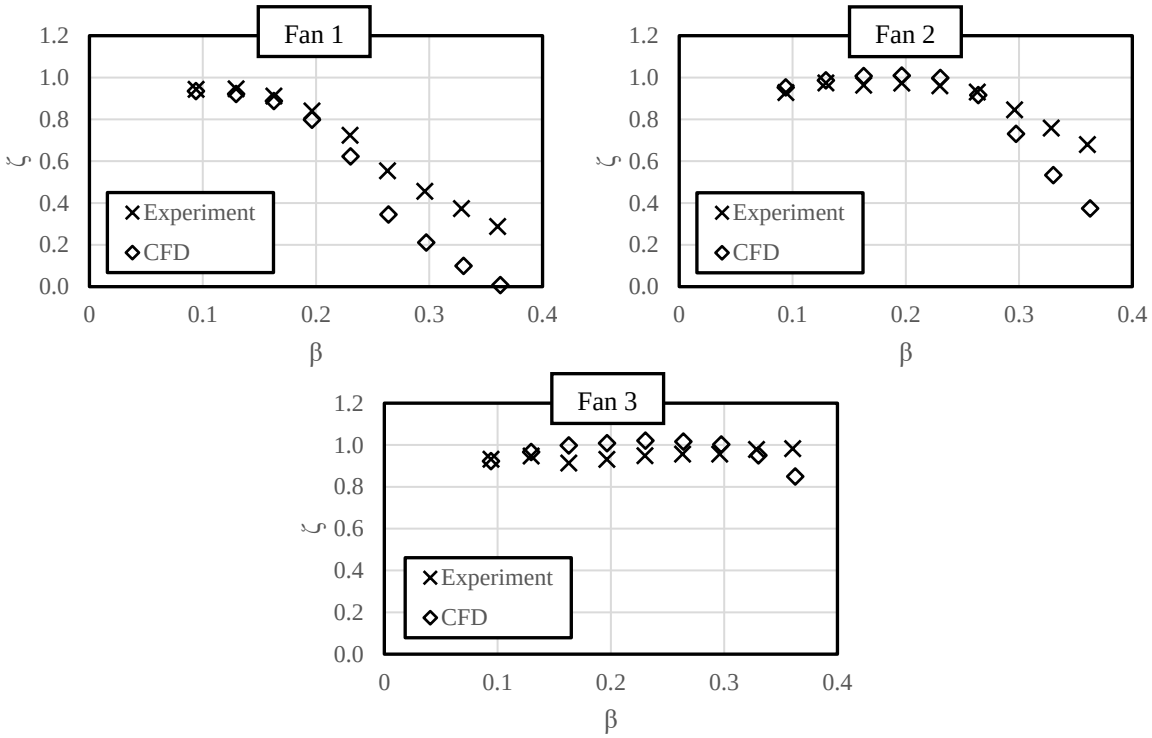

Figure 5: Effect of cross-flow on individual fan performance – Screen 25% coverage

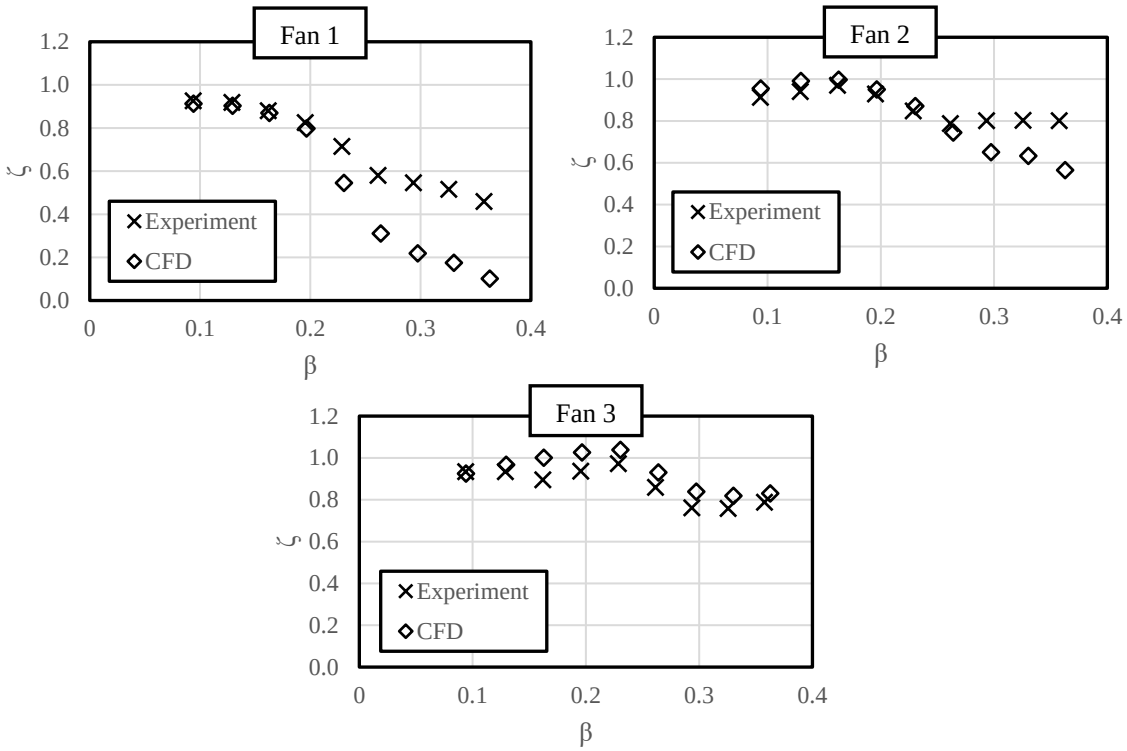

Figure 6: Effect of cross-flow on individual fan performance – Screen 50% coverage

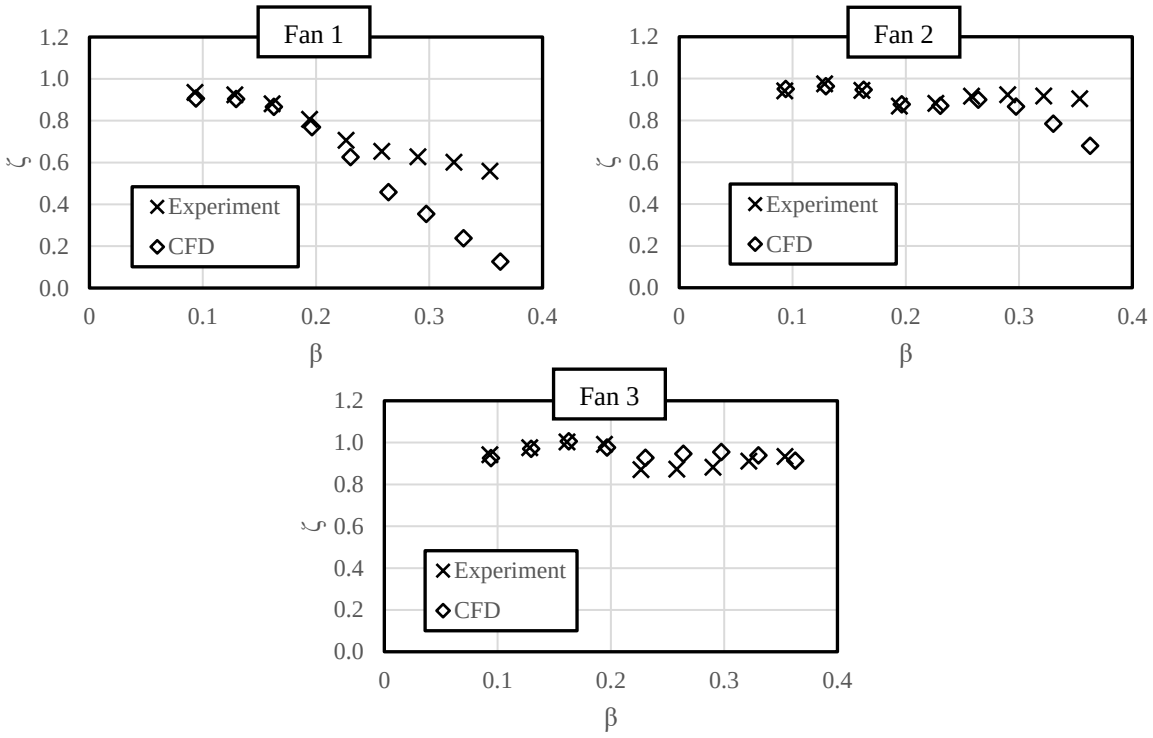

Figure 7: Effect of cross-flow on individual fan performance – Screen 75% coverage

The numerical model demonstrates the ability to quantitatively represent fan row performance for moderate cross-flow conditions. Fig. 8 shows that in terms of system volumetric effectiveness, described by Eq. (8), the numerical model is able to predict the investigated experimental cases within a maximum error (Eq. (9)) of 4% up to β = 0.25 (speed at platform height ~ 6 m/s, Eq.7, equating to 9 m/s at full-scale). At higher cross-flow conditions, only a qualitative evaluation is offered, within a maximum error of 24% up to β = 0.35 (speed at platform height ~ 11 m/s, 16 m/s full-scale)

$$\zeta_{sys} = \sum_{i=1}^{3} \dot{V}_{actual,i} / \sum_{i=1}^{3} \dot{V}_{ideal,i} \quad (8)$$

$$\text{Error} = \text{abs}\left[\zeta_{sys,CFD} - \zeta_{sys,EXP}\right] / \zeta_{sys,EXP} \quad (9)$$

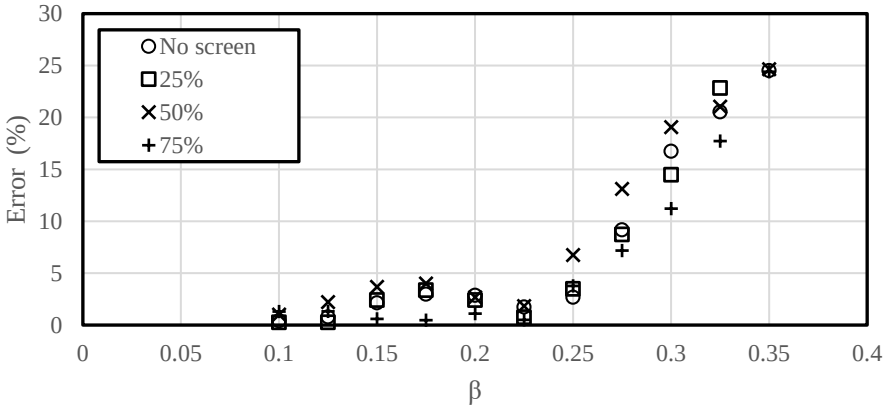

Figure 8: CFD model error quantification

4 ANALYSIS OF SCREEN EFFECTS AND DISCUSSION

An assessment of the screens in terms of system volumetric effectiveness is given in Fig. 9. For the particular case investigated, characteristic of an ACC of low platform height, the inclusion of peripheral windscreens is observed to have a primarily negative effect on fan performance relative to when no windscreen is present, with a maximum performance deficit of up to 19% determined with a screen at 50% coverage at $\beta = 0.26$ (approximated full-scale wind speed at platform height of 10 m/s)

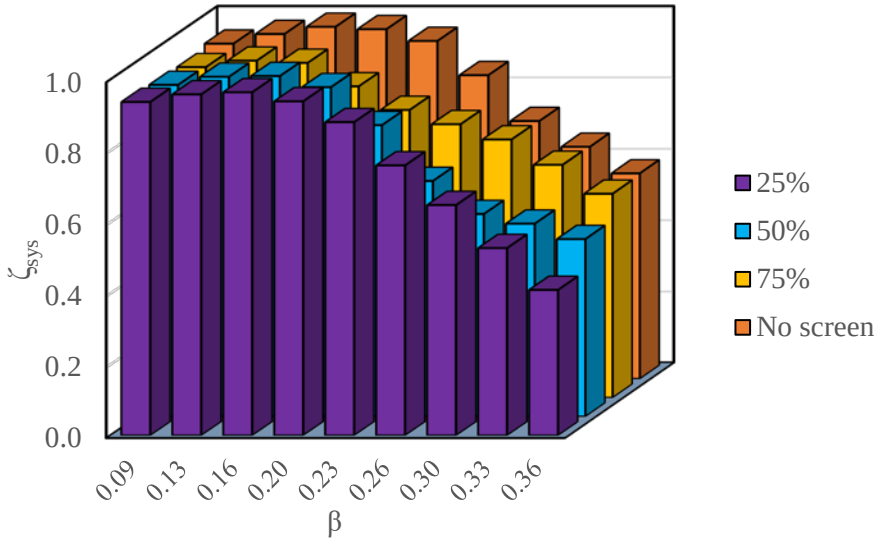

Figure 9: Effect of screens on system volumetric effectiveness

Causes for the reduced performance is accredited to the exacerbation of the low pressure region that develops at the peripheral inlet of the fan row further downstream, shown in Fig. 10. The screens constrict the peripheral inlet area, forming an accelerated flow region beneath them, as shown in Fig 11, causing a deficit of flow in the wake of the screens.

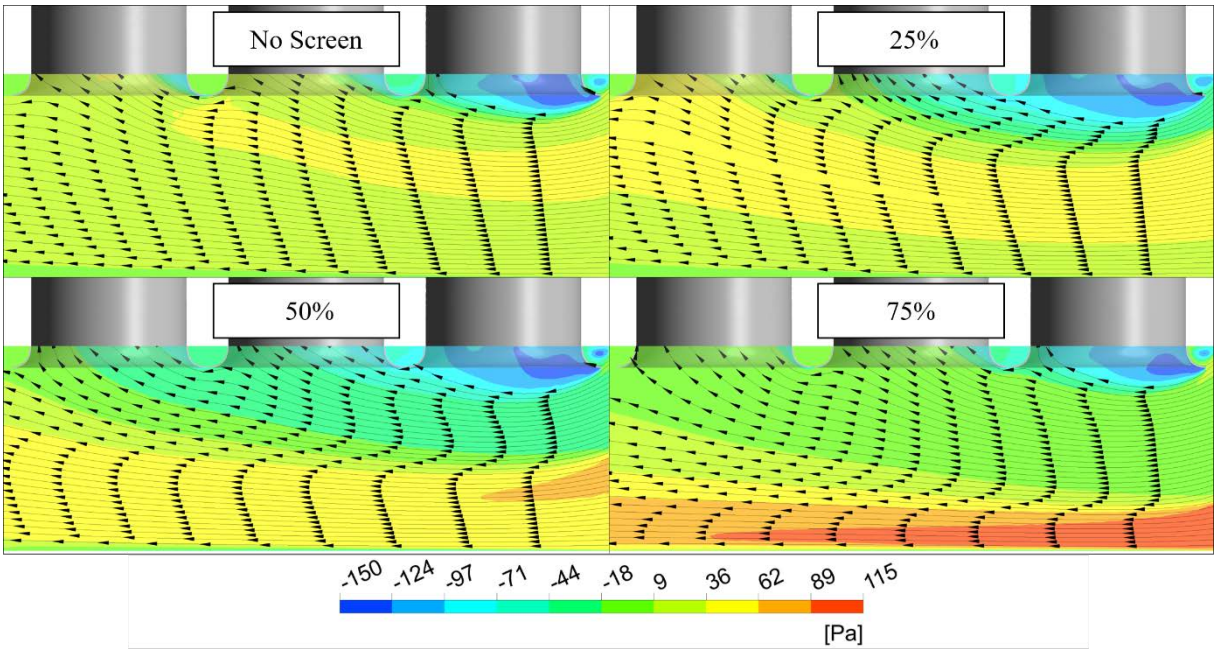

Figure 10: Total pressure contours beneath fan row with screens at different percentage inlet coverage, $\beta = 0.3$

Slight performance enhancement is, however, observably offered at very high cross-flow rates ($\beta > 0.3$, ~ 8 m/s, Eq. 7) when the screen covers a high percentage of the peripheral inlet area. At high cross-flow rates the accelerated flow region effectively bypasses the fan row, enabling the formation of a low speed flow region ahead of the 2nd and 3rd fan, which raises the static pressure beneath the fan row. Flow is more axially entrained into these fans, causing a subsequent shrinkage of the low pressure region ahead of the 1st fan. Furthermore, the screens are found to produce more uniform inlet velocity profiles, which has a favourable consequence on dynamic blade loading, an assessment still underway as part of this on-going study.

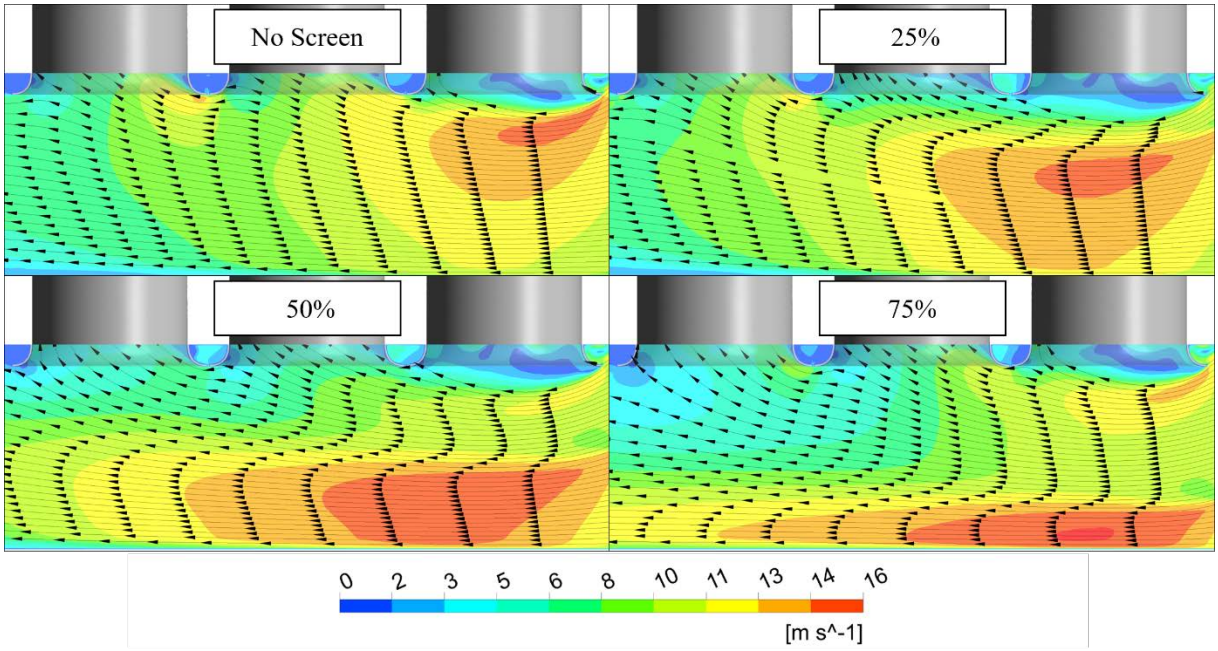

Figure 11: Velocity magnitude contours beneath fan row with screens at different percentage inlet coverage, $\beta = 0.3$

CONCLUSION

A validated numerical ACC fan row model that can be used to explore peripheral windscreen effects on fan performance is presented. Quantitative prediction of fan row performance, in terms of system volumetric effectiveness, is found to be realizable for moderate cross-flow conditions (< 10 m/s, full-scale), while only qualitative prediction is offered thereafter due to the limitations of the implicit fan models. The numerical model replicates the experimental facility used by Marincowitz (2018) and for the particular case, the installation of peripheral windscreens has a primarily negative effect on fan performance. The reduction in fan performance is attributed to the development of a low pressure wake behind the screens and ahead of the fan intakes. The results within this study are, however, limited due to the two-dimensional flow approximation upon which the replicated experimental fan row facility is based. It is assumed that flow only enters the fan row from the peripheral inlet and that the sides of the fan row can be treated effectively as symmetry planes. The current numerical model, therefore, does not make provision for the inclusion of possible edge effects that may alter the drawn conclusions. The results of this study are further limited to only the particular case investigated, as the influence of platform height needs to be reviewed. This model, however, provides a reliable tool for future, more complex or generalizable iterations. The model is also

suited for the investigation of ACC fan blade loading effects, which is still underway as part of this on-going study.

ACKNOWLEDGEMENTS

The authors acknowledge the financial support provided by the National Research Foundation (NRF) and Howden Netherlands B.V.

REFERENCES

Augustyn, P.H. (2013). *Experimental and Numerical Analysis of Axial Flow Fans.* University of Stellenbosch.

Fourie, N. (2014). *Simulating the effect of wind on the performance of axial flow fans in air-cooled steam condenser systems.* University of Stellenbosch.

ISO (2007) 'INTERNATIONAL STANDARD ISO 5801 Industrial fans –Performance testing using standard airways'.

Lewis, R.I. (1996). *Turbomachinery performance analysis.* London: Butterworth and Heinemann.

Marincowitz, F.S. (2018). *Experimental investigation of the effects of windscreens on air-cooled condenser fan performance and dynamic blade loading*, University of Stellenbosch.

Maulbetsch, J. S., DiFilippo, M. N. and O'Hagan, J. (2011). 'Effect of Wind on Air-Cooled Condenser Performance'. In: *Proceedings of the ASME 11th International Mechanical Engineering Congress & Exposition*, Denver, Colorado.

Maulbetsch, J. and DiFilippo, M. (2016). *The use of Wind Barriers to mitigate the effect of wind on air-Cooled Condensers.* doi: CEC-500-2016-047.

Meyer, C. J. (2004). 'Numerical investigation of the effect of fan performance on forced draught air-cooled heat exchanger plenum chamber aerodynamic behaviour', *Applied Thermal Engineering*, 24, pp. 359–371.

Shih, T., Liou, W.W, Shabbir, Z.Y. and Zhu, J. (1995). 'A new k- ε eddy viscosity model for high Reynolds number turbulent flows', *Computers Fluids*, 24(3), pp. 227-238.

Stinnes, W. H. and Von Backström, T. W. (2002). 'Effect of cross-flow on the performance of air-cooled heat exchanger fans', *Applied Thermal Engineering*, 22(12), pp. 1403–1415.

Thiart, G.D. and von Backström, T.W. (1993). 'Numerical simulation of the flow field near an axial flow fan operating under distorted inflow conditions', *Journal of Wind Engineering and Industrial Aerodynamics*, 45, pp. 189-214.

van der Spuy, S. J. (2011). *Perimeter Fan Performance in Forced Draught Air-cooled Steam Condensers*. University of Stellenbosch.